Received: 30 April 2022 | Revised: 25 November 2023 | Accepted: 12 February 2024

DOI: 10.1002/esp.5809

RESEARCH ARTICLE

ESPL WILEY

The impacts of low flow, ice-cover and ice thickness on sediment load in a sub-arctic river – Modelling sediment transport with particle image velocimetry calibration data sets

Virpi Pajunen[1,2] | Eliisa Lotsari[1,2] | Juha-Matti Välimäki[1,2] | Franziska Wolff[1] | Marko Kärkkäinen[1] | Linnea Blåfield[3] | Anette Eltner[4]

[1]Department of Geographical and Historical Studies, University of Eastern Finland, Finland

[2]Water and Environmental Engineering, Department of Built Environment, Aalto University, Finland

[3]Department of Geography and Geology, University of Turku, Finland

[4]Institute of Photogrammetry and RemoteSensing, Technische Universität Dresden, Germany

Correspondence
Virpi Pajunen, Department of Built Environment, Aalto University, Otakaari 1B, P.O. Box 11000, FI-00076 AALTO, Espoo, Finland.
Email: virpi.pajunen@aalto.fi

Funding information
Academy of Finland, Grant/Award Numbers: DefrostingRivers, 338480, ExRIVER, 267345, HYDRO-RDI, 337279, 337394

Abstract

Climate change will be pronounced in sub-arctic and arctic regions. Consequently, a shorter ice-cover period, increased precipitation and changes in the timing and magnitude of discharge are expected. These hydroclimatic changes can have an impact on sediment transport in northern rivers. Studying spatial and temporal variation of the processes in low-flow open-water and ice-covered conditions is crucial to improve the prediction of future changes. The investigation of under-ice conditions has been challenging and new approaches for their measurement are much needed. We analyse the spatial sediment transport in a meandering subarctic river during different flow conditions, i.e., low flow open-channel during autumn and ice-covered during winter. We use one-dimensional (1D) morphodynamic models with image-based sediment transportation data sets. We also simulate sediment transport with different ice thicknesses to better understand the overall bedload transport in a sub-arctic river in mid-winter conditions.

Simulations for the studied meander bend showed a considerable flow-driven decrease of sediment transport in ice-covered conditions when compared to open-water conditions. Erosion was more pronounced in open-water conditions and deposition was the prevailing process in ice-covered conditions. When an additional increase in ice thickness was simulated, bedload increased, because the thicker ice narrowed the river channel substantially and thus leading to an increase in flow velocity and shear forces. Instead of solely relying on the sediment samples, the additional consideration of an image-based sediment data set enabled a more reliable model calibration in ice-covered conditions. This encourages further usage of image-based methods for sediment transport estimations, especially in ice-covered conditions. In the future, changes in river-ice can be expected to decrease under-ice sediment load but increase annual open-water sediment loads. The increasing summative sediment transport of small arctic and subarctic rivers can have significant consequences on the downstream waterbodies.

KEYWORDS
Finland, ice-covered flow, image processing, modelling, sediment transport, subarctic

1 | INTRODUCTION

Climate change alters hydroclimatic conditions, especially in high latitudes (IPCC, 2021). Anticipated changes include shorter ice-cover periods, increased annual precipitation and more intensive storm events. These changes have an impact on river flow conditions. Sediment transport is predicted to increase with increasing discharge (e.g., Boyer et al., 2010; Lotsari et al., 2014; Verhaar et al., 2011) and the annual bedload transport may increase further as ice-cover periods become shorter in the future (Prowse et al., 2011). In subarctic and arctic regions, the impact of diminishing river-ice can be more pronounced, because currently the ice-covered period still lasts up to eight months (Lotsari et al., 2015). Furthermore, high-magnitude discharge events may increase erosion. However, these events are still temporally brief compared to low discharge conditions. During low flow conditions, erosion forces may be lower, yet they still contribute to the long-term impact of sediment transport to the downstream water bodies (Leopold, Wolman, & Miller, 1964; Lotsari et al., 2014). In sand-bed systems, the cumulative load during the low flow season can be greater than the load caused by peak flow conditions (Lotsari et al., 2014). More studies on low-flow sediment transport are required, especially in ice-cover conditions.

The understanding of climate change's effects on water bodies demands robust estimations of annual sediment transport during current and projected conditions. The information on spatial and temporal variation of the processes under ice-covered conditions is insufficient, which limits the understanding of subarctic river dynamics (Ettema, 2002; Lotsari et al., 2019; Turcotte et al., 2011). Under-ice flow velocities are usually lower compared to open-channel conditions because the water-ice boundary reduces the water velocity due to friction (Ettema & Kempema, 2013; Lotsari et al., 2017). Consequently, a stable ice-cover also reduces the river channel's sediment transport capacity (Turcotte et al., 2011). However, the impact of ice-cover on flow and sediment transport may vary depending on the river-ice conditions. Laboratory studies have found that freely floating ice-cover, i.e., not attached to riverbanks, does indeed decrease the bulk flow velocity due to increased friction (Ettema, 2002; Smith & Ettema, 1995; Sui et al., 2010; Tsai & Ettema, 1996). But if the ice-cover is thick and fixed to the banks, the bulk flow velocity is forced to increase (Ettema, 2002). Robert & Tran (2012) detected in their experiment higher maximum velocities in ice-covered conditions when compared to open-water conditions. In field studies of natural rivers, under-ice flow velocities and discharge have been found to be slower than in low-flow open-water conditions. However, the ice-cover also affects the distribution of flow velocities in the river channel, which may have implications for sediment transport under ice (Lotsari et al., 2017, 2019).

Over time, studies conducted either in the laboratory (Ettema, Braileanu, & Muste, 2000; Lau & Krishnappan, 1985; Muste, Braileanu, & Ettema, 2000; Sayre & Song, 1979) or in natural rivers (Kämäri et al., 2015; Lotsari et al., 2019) have found that sediment transport declines in ice-cover conditions. In a meandering sub-arctic river, total erosion was lower in ice-covered conditions when compared to the low-flow open-water period, yet there was more spatial variability among depositional and erosional locations in ice-covered conditions (Lotsari et al., 2019). Studies related to future hydroclimatic scenarios and their impacts on in-channel sediment transport have simulated increased discharges and therefore greater erosion forces especially in winter (e.g., Boyer et al., 2010; Verhaar et al., 2011), while in other seasons deposition may be the more predominant process in the future (Lotsari et al., 2014). Kämäri et al. (2015) observed that a river in south-western Finland ice-cover mainly reduced erosion, but hydro-morphological simulations with rough ice (roughness value, Manning's $n = 0.04$) estimated an increase of erosion in parts of the river channel, where the thick ice substantively decreased the conveyance of the channel.

The lack of robust calibration data for sediment transport models in ice-covered conditions hinders a reliable sediment load estimation. Traditionally used measuring methods of bedload (e.g., mechanical samplers, such as those created by Helley & Smith, 1971) provide vague snap-shot estimations of sediment transport and are difficult to constrain even in open-water conditions (Polvi et al., 2020). Too short measurement times do not capture flow pulsations, which can play a significant role in sediment transport (Demers, Buffin-Bélanger, & Roy, 2013; Lotsari et al., 2020a). Additionally, hydraulic and trap-efficiency tests of mechanical samplers showed over-registration of sediment load in low-flow conditions and in streams carrying sand-sized material (Helley & Smith, 1971). In ice-covered river conditions, measurements are done through holes in the ice, and hence, the obtained data consists of merely point measurements (Demers, Buffin-Belanger, & Roy, 2011; Lotsari et al., 2017). Existing studies lack direct, continuous, high-resolution measurements of flow and sediment transport (Polvi et al., 2020).

Models that estimate bedload transport rely on the quantity and quality of calibration data (e.g., topography, flow, bedload data) measured in the field. To enhance the model calibration, in clear water conditions image-based velocity measurement methods (e.g., Eltner, Sardemann, & Grundmann, 2020; Perks et al., 2020) can give insights into the velocity of the sediment moving along the riverbed. Furthermore, image-based approaches can provide information about the load, when evaluating the speed and characteristics of the sediment (Ancey & Pascal, 2020).

Open-access software (e.g., HEC-RAS) for the simulation of hydraulics and sediment transport enable 1D and 2D hydro-morphological modelling. Due to the complexity of the processes, 1D modelling approaches are more cost-efficient for ice-cover scenarios (e.g., Kämäri et al., 2015). Some of the open-source 2D and 3D numerical models (Mosselman, 2012) already have some basic ice modelling features included (Goede et al., 2014) or can account for ice processes using an external model (Oveisy et al., 2015). Although some open-source 2D models include ice-cover, they do not yet include sediment transport processes (Lotsari et al., 2019) highlighting the need for further development.

This study aims to 1) analyse the spatial sediment transport with 1D morphodynamic models in low-flow open-channel conditions during autumn and ice-covered flow conditions during winter, 2) test whether the winter sediment transport models can be enhanced using image-based calibration data and further 3) to simulate how different ice thickness conditions in wintertime are expected to affect the sediment transport. The variability of the bedload transport will be defined based on the measured maximum and minimum ice-thickness and no-ice conditions to better understand the overall bedload transport in a subarctic river in mid-winter conditions. In addition to mechanical bedload samples during autumn and winter, the winter

bedload calibration is supported by under-water photogrammetry to define the bedload velocity and its amount. The accuracy of models using different calibration data (e.g., photogrammetry vs traditional mechanic models using Helley-Smith) is compared.

2 | METHODOLOGY AND METHODS

2.1 | Study area

The meandering upper Pulmanki River is located in northern Finland (Lapland; Figure 1). It is a tributary of the Tana River, which is a border river between Finland and Norway, that further drains into the Arctic Sea. According to Peel, Finlayson, & McMahon (2007), the area belongs to the cold climate category, with cold summers without a dry season. Maximum discharges occur during the spring snow-melt period (discharges up to 50 m^3s^{-1}: Kasvi et al., 2013). However, during the summer season (from June to August) rain-induced high discharge events also occur causing erosion (Lotsari et al., 2020b). The water level variation during the open channel period, i.e., between the spring peak and the low water period before the freezing conditions in autumn, can be more than 2 m (Lotsari et al., 2010; Lotsari et al., 2020a). The discharge is lowest in mid-winter (February–March), for example, measured as 0.63 m^3s^{-1} in early March of 2014 (Lotsari et al., 2019). Thus, the hydro-climatic variations are large between seasons. Often from October to April (i.e., for seven months), sub-zero winter air temperatures, ice-cover and low discharges impact the river (Lotsari, Lind, & Kämäri, 2019).

The Pulmanki river channel is highly meandering with wandering mid-channel bars. The studied river reach consists of a symmetric meander bend. The sediment, which is glacio-lacustrine and glacio-fluvial in origin (Hirvas et al., 1988), is highly mobile and erodible (Lotsari, Lind, & Kämäri, 2019). The D_{50} values of the riverbank materials are between 0.004 mm and 0.529 mm (Lotsari et al., 2020b), and

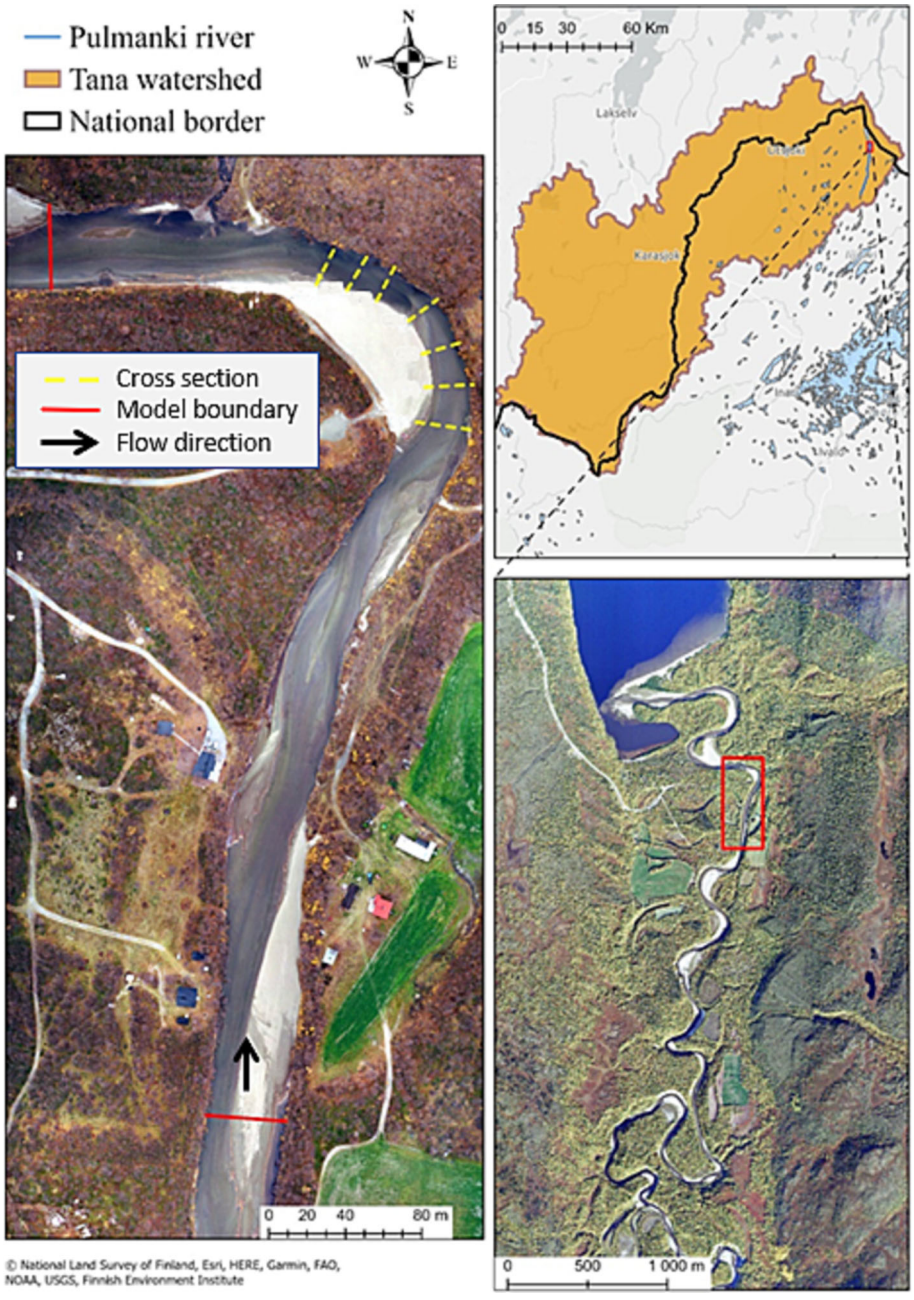

FIGURE 1 The meandering Pulmanki River is located in northern Finland close to the Norwegian border in the Tana watershed (top right), the location of the model area in Pulmanki River (bottom right) and the cross-sections, model boundary locations and flow direction (left). The names of the cross-sections from upstream to downstream are CS1, CSA, CS2, CSB, CS3, CSC and CS4.

the riverbed materials' D_{50} values are between 0.427 mm and 0.788 mm (Lotsari et al., 2020a) and 0.448 mm and 1.456 mm (this study). The sediment is transported mainly as bedload during autumn and winter. The water turbidity was negligible during the study period, indicating non-existent suspended transport. Due to the transparent water, the riverbed forms can be seen clearly in the (aerial and underwater) images used for the photogrammetric processing. The measurements were carried out for this study during two field campaigns: one in September 2020 and one in February 2021. The February measurements represent the mid-winter and ice-covered low-flow period.

2.2 | Hydrological and hydraulic data

The discharge and flow velocities were measured with Sontek's Acoustic Doppler Current Profiler (ADCP, M9 sensor) during both field campaigns in September 2020 and February 2021. The accuracy of the sensor is +/− 0.25% of measured velocity (+/− 0.2 cms^{-1}). It has four 3.0 MHz beams and four 1.5 MHz beams (Sontek, 2024). The depth is measured with the sensor's vertical beam. In addition to the discharge, the provided data at each measurement location include flow velocity, flow direction and water depth throughout the water column.

During the autumn low water period, the sensor was mounted on a Sontek hydro-board and pulled across the river with ropes attached to both sides of the platform. The measurements were done in seven cross-sections, starting from cross-section CS1 (upstream) and ending with cross-section CS4 (downstream) (Figure 1). The cross-section names follow those used in previous studies at Pulmanki River (i.e., four main cross-sections CS1-4 and three additional cross-sections [CSA, CSB and CSC] located between the main cross-sections). The sensor measured in the moving-boat mode. Transducer depth was 0.06 m and the temperature correction was set for a water temperature of 8.1°C (YSI measurement). The discharge and water depth were measured on the 15th of September at CS1, i.e., the most upstream cross-section at the meander bend (average discharge 2.192 m^3s^{-1} and depth 0.282 m), and at the upstream boundary of the modelling area (see Figure 1) on 18th of September (average discharge 3.239 m^3s^{-1} and depth 0.555 m).

During winter, the sensor was applied in stationary mode, and the mid-section method was selected for discharge calculations. The same seven cross-sections were investigated by drilling holes into the ice-cover such, that each drill hole was 1 m apart. The sensor, which was mounted on a metal rod, was lowered through the ice holes to the level of the ice-water interface. A transducer depth of 0 m was used to measure the whole water column, including the turbulence possibly caused by the ice-cover. The water temperature was 0°C. Before each cross-sectional ADCP measurement, the tagline azimuth was defined. The averaging time for the mid-section method was set at 60 s for each measurement station, i.e., drill hole. The discharge on the 15th of February was 0.397 m^3s^{-1} at CS1, where the flow entered from the straight reach and the curvature of the meander bend did not yet have any influence.

The water level and the height of the river ice surface were measured with RTK-GNSS (Trimble R10) at each measurement location. In addition, the ice thicknesses were measured at each drilled hole. In some of the drill holes, the ice was frozen to the riverbed. These locations were also measured for modelling purposes (see below).

During the autumn field measurements, the Solinst Levellogger pressure sensor (for depth values at 15 intervals) was located at the upstream boundary of the study area. In addition, the water level was measured at the upstream and downstream boundaries with RTK-GNSS. The difference in water level between these locations was 0.299 m on the 16th of September (both measurements were taken within 15 min). As there was no water depth data from the downstream boundary, the RTK-GNSS water level measurements of the upstream boundary were related to the water depth data of the pressure sensor from the 15th to the 19th of September. Thereby, the water levels of the downstream boundary were then calculated by subtracting the 0.299 m from the upstream boundary's water levels. The measured discharges were related to the water levels at the time of these measurements (on the 15th and 18th of September). A linear regression was performed between the upstream-downstream discharge-water level value pairs to calculate the discharge at 15 min intervals. This allowed us to define the discharge and water level during the period of the bedload measurement and to use the data as the boundary conditions of the autumn open-channel flow model.

In addition to the ice thickness measurements in February 2021, there was long-term mid-winter ice thickness data available for the years 2014–2021. Based on this data, the maximum ice thickness was 64 cm at a drill hole of the upstream cross-section (2014). The minimum ice thickness measured was 14 cm in 2016. These values were used for the modelling.

2.3 | Sediment transport data

Water samples of 500 ml were taken during the sampling periods in autumn and winter. In the laboratory, turbidity (FTU: Formazine Turbidity Unit) and colour (Pt, mg/l) were measured with a YSI 9500 photometer of a Xylem brand. Also, total suspended solids (TSS, mg/l) were analysed (see Appendix, Table A1). The vacuum filtering was performed using filters with nylon pore sizes of 0.45 µm (Whatman® membrane filters diameter 47 mm). The empty filters had been dried (at 105°C) and weighed before filtering 200 ml of water through them. The filters were then again dried at the same temperatures, placed in an exicator for at least one hour and then weighed. The weight of the empty filters was subtracted from these sampled filters.

The Helley-Smith sampler (Helley & Smith, 1971) was applied to mechanically measure the bedload transport on the 19th of September 2020 and 18th of February 2021. The intake opening of the sampler was 77 mm. The sampling period lasted six minutes, except for the first sample on the 19th of September, which took 3 minutes (Appendix, Table A2). The samples were dried in the oven (105°C) and weighed. The grain size distributions were analysed via dry-sieving, and the D_{50} values were calculated (Table A2). The average D_{50} value of all bedload samples was 0.79 mm in autumn, and 0.54 mm in winter. Thus, 31.5% smaller particles were transported in winter conditions compared to autumn.

During winter, the GoPro HERO9 Black action camera was used to capture still-images and video clips from the ice-holes of CS1. Therefore, targets were inserted through a diamond-shaped hole sawed into the ice, which covered roughly 1 m × 1 m and was

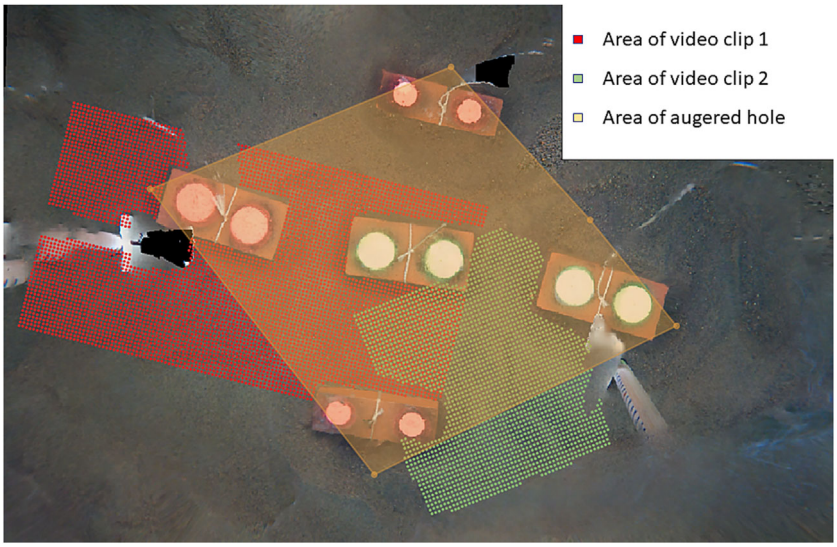

FIGURE 2 An image of the under-ice photogrammetry study setting taken with GoPro HERO9 Black action camera. The image shows the targets on the riverbed, the areas of the two video clips used in the analyses and the area of the augered hole in the ice.

positioned in such a way that it was possible to hold a survey rod vertically (Figure 2). Then, the camera was attached to a rod, inserted through the hole and moved around in the river water trying to cover the area of interest from every angle while capturing video clips. The most suitable frames for photogrammetric 3D reconstruction were selected from the video clips. The data was used to create a digital elevation model and an orthoimage of the riverbed using Structure from Motion (SfM) and to calculate the mean bedload transport velocity using large-scale particle image velocimetry (LSPIV; Fujita, Muste, & Kruger, 1998). Targets measured with RTK-GNSS were inserted close to the riverbed so that the resulting digital elevation model and orthoimage could be georeferenced. Processing was done in Agisoft Metashape Professional (version 1.7.5.13229).

To apply the image velocimetry method using LSPIV, the videos were captured with a resolution of 1920 × 1,080 pixels and a frame rate of 120 frames per second. The lengths of the two utilized video clips were 15 seconds. The clips captured two locations (Figure 2). Since the videos were not recorded in a systematic way, i.e., moving around a lot, suitable video clips had to be selected by visual inspection and test runs with LSPIV. Two criteria for the selection were considered. A camera position of near (nadir view relative to the riverbed to enable accurate scaling of the measurement) and a relatively still video capture so that the co-registration of video frames to the first frame of the same clip was possible to correct camera movements between frames (e.g., Ljubičić et al., 2021).

LSPIV processing was done in Matlab using the add-on tool PIVLab (Thielicke & Stamhuis, 2014). The extracted video frames were undistorted before processing, using the camera calibration parameters that were estimated during the 3D reconstruction in Agisoft Metashape. The sparse distribution of moving particles and the pulsating nature of bedload transport complicated the analysis because the image velocimetry -method relies on average velocity values. Thus, if frames captured events of fast bedload transport but also periods of only minimal particle movements, the mean bedload velocity would be significantly underestimated. Therefore, the videos had to be cut to short clips (1–10 seconds), where movement was most visible. The video frame extraction rate (i.e., the number of frames per second considered from the original video) also affects the calculated mean velocity values due to the settings of LSPIV parameters (mainly search window size) and the amount of movement in pixels between frames. For instance, if too many frames per second are extracted and thus considered for the processing of low particle velocities, no movement between consecutive frames might be detected destabilizing the velocity estimation. Different combinations of LSPIV settings and frame extraction rates were tested. The final mean bedload velocities were calculated using a frame rate of 30 frames per second and applying the two-pass FFT calculation with an initial search window size of 64 pixels and a 50% step size.

The raw mean velocity values (pixels per frame) were scaled to meters per second considering the ground sampling distance (pixel per meter) and timestep between frames (second). Finally, the velocities were georeferenced using the orthoimage and digital elevation model.

The mean bedload transport velocity (us,m) was needed to calculate the mean bedload transport rate (q_b) using the simplified bedload transport rate equation (equation 1, Zanke & Roland, 2020), assuming that the moving effective bedload layer (s_b [m]) is one-grain diameter thick. The average D_{50} value from the Helley-Smith measurements was 550.3 μm. The bedload transport rate (q_b [m^2s^{-1}]) was transformed to make it comparable to the Helley-Smith measurements (kg m^{-1} s^{-1}) by multiplying it with the density of the transported material, which was assumed to be the one of quartz (2.65 gcc^{-1}) (Zanke & Roland, 2020).

$$q_b = u_{s,m}{}^{*} s_b \quad (1)$$

where q_b is the mean bedload transport rate (m^2s^{-1}), $u_{s,m}$ is the sediment transport velocity (ms^{-1}) and s_b is the effective thickness of the moving bed-load layer (m).

The bedload data were applied together with the Helley-Smith data to verify sediment transport models for the winter period.

2.4 | Bathymetry

The bathymetry estimation for the autumn period was largely based on the UAV data introduced by Eltner et al. (2021). The UAV data was collected simultaneously with the other field measurements in

September 2020. The calculated bathymetry was verified with RTK GNSS measurements and the cross-sectional ADCP data from the 15th of September. These measurements revealed that the riverbed heights at the outer bank's deepest sections were slightly overestimated by the UAV approach. The bathymetry was refined with the ADCP and RTK-GNSS measurements for areas where the elevation of the ADCP measurements differed from the UAV-based bathymetry.

The winter bathymetry was created by refining the autumn UAV bathymetry data. The estimated riverbed elevations based on water depth, ice thickness and RTK-GNSS measurements at the cross-sections were used to adjust the bathymetry. The areas between the cross-sections were approximated and regions were adapted, where the elevation of the winter riverbed differed from the autumn bathymetry.

The height values of the river channel bed from autumn 2020 and winter 2021 were compared to each other. In total, 74 points were found, where the bathymetry differed more than 5 cm. The mean absolute difference was 17.8 cm. The normal distribution of the difference of the height values was tested by a Shapiro–Wilk test. Based on the test difference, the autumn and winter height values were normally distributed ($W = 0.97149$, p-value $= 0.09252$). The paired t-test was then used to test the difference between the autumn and winter height values. The differences statistically significant ($t = 4.3605$, $df = 73$, p-value $= 0.0004$). Based on the comparison of the height values the riverbed had changed in the meander bend area between autumn and winter. Due to the change, a new bathymetry was estimated for the winter period approximating the areas between cross-sections based on the measurements at the drilled ice holes. Height values from autumn were used at a thin part in the inner bank of the bend for the winter data. In this area, ice was frozen to the riverbed, and it had been under minimum fluvial effect. Thus, it was assumed to represent the autumn conditions. Finally, the bathymetry was interpolated for the whole meander bend area for the winter models. The interpolations were implemented by the "topo to raster" method using the software ArcGIS Pro (version 2.9.0).

2.5 | Hydraulic model build-up and calibration

The hydraulic and morphodynamic modelling was done with HEC-RAS 6.1, which is a river analysis software developed by The U.S. Army Corps of Engineers. HEC-RAS allows sediment transport-mobile bed modelling and incorporates river ice conditions.

The open-water model was based on topography and bathymetry derived from the ADCP and UAV data captured during autumn. The modelling area was a 650 m-long river segment encompassing seven cross-sections (cf. Figure 1). The hydraulic model was created by performing an unsteady flow analysis with a steady mode. The unsteady analysis was chosen, because it solves the continuity and momentum equations simultaneously for each cross-section (Brunner, & Savant., G., Heath, R.E., 2020). Upstream discharge ($Q = 4.324$ m^3s^{-1}, at the upstream boundary, estimated from the upstream boundary water level) and downstream water level ($WL = 13.986$ m, at the downstream boundary) were used as boundary conditions. They were set as constant during the simulations. Water temperature was set to 5.86°C and it was based on level logger data at the upstream boundary (24 h average from 19.9.2020). The model was run for a 24 h simulation period considering a 1 h warm-up. The computational interval was set to 5 seconds to ensure more reliable calculations (Brunner, & Savant., G., Heath, R.E., 2020).

The Manning roughness coefficient (Manning's n) of flow resistance was used as the calibration parameter of the hydraulic model. It was adjusted before each model run. The modelled water levels at each cross-section were then compared with the measured values and assessed with the Root Mean Square Error of Prediction (RMSEP), the Mean Absolute Error (MAE) and the Coefficient of Determination (R^2). The best model was reached with Manning's $n = 0.02$ (Table A3).

The hydraulic model of ice-cover was based on topography and bathymetry created for the winter period. The same modelling area was used as in the autumn model. The ice-cover data was entered for each cross-section (i.e., the mean ice-cover and ice-cover thickness calculated from the drillhole measurements at each cross-section), and the upstream and downstream model boundaries (cf. Figure 1) were extrapolated, correspondingly. Upstream discharge ($Q = 0.397$ m^3s^{-1}, at the upstream boundary) and downstream water level ($WL = 14.313$ m, at the downstream boundary) were set as boundary conditions. The discharge for the upstream boundary condition was derived from the nearest cross section (CS1). The water level for the downstream boundary was extrapolated from the drillhole data. The water temperature was set to 0°C. The unsteady flow analyses were run with the same settings as for the autumn model.

The winter model was calibrated using the measured water depth (under ice), the water level of the ice-top surface and the mean velocity data at the cross sections. The Manning roughness coefficient of both riverbed and ice were used as the calibration parameters. They were adjusted before each model run. The modelled and measured values were compared and assessed with RMSEP, MAE and R^2. The best models were reached with an ice roughness of 0.01 and a riverbed roughness of 0.02 (Table A4).

2.6 | Morphodynamic model construction and calibration

The best hydraulic models were selected to perform the sediment modelling. For the autumn model, bed gradation data was collected in autumn 2020 with the Van Veen grab sampler. These bulk sediment samples were taken at all seven cross-sections, at the inner, middle and outer banks. From all samples, 500 g of sediment was dry sieved (using a similar dry sieving procedure as in the case of the Helley-Smith samples), except for the middle sample from CS4 (386.8 g). The average D_{50} of the samples was 0.569 mm. Based on the three samples of each cross-section, mean percentages were calculated for each grain class at each cross-section.

These mean percentages of grain sizes were used for each cross-section and values were interpolated for the upstream and downstream boundaries which had no bed gradation data. The equilibrium load was set as the boundary condition for the sediment load. The equilibrium load is used to compute the boundary sediment load from the bed gradation and the transport capacity. The equilibrium sediment transport capacity is computed at the upstream cross-section and these capacities are then introduced as a cumulative load into the

next cross-section (US Army Corps of Engineers, 2021). Initial conditions and transport parameters were set to Copeland (Ex7) for the sorting method and Van Rijn for the fall velocity method. For the Wilcock and Crowe transport function, the Active Layer was selected. Copeland (Ex7) is an alternative version of the Thomas mixing algorithm (Exner 7), which Copeland (1993) designed for rivers with sand beds. It forms armour layers more slowly and thus calculates more erosion. The transport function was used as a calibration parameter for the sediment model. Eight different transport functions (i.e., Ackers and White, Engelund and Hansen, Copeland's form of Laursen (Laursen-Copeland, LC), Meyer-Peter and Müller (MPM), Toffaleti, MPM-Toffaleti, Yang and Wilcock and Crowe) were used for the calibration because they all were justified as they had been developed for silt, sand and sand-gravel beds (Table 1).

The transport model parameters were set to continuity for the routing method. The sediment junction split method was chosen as flow-weighted. The upstream capacity was set as pool pass-through method. Then, unsteady flow analyses were run considering sediment and using the same model settings as for the best hydraulic model. The analysis was repeated for each transport function. The sediment models were calibrated against the measured average sediment load (kg day^{-1} m^{-1}) at CS1, which was calculated from the Helley-Smith samples (Table 2).

Based on this initial calibration, the most suitable transport function, i.e., MPM, was selected for further modelling. MPM is a bedload equation based on a simple excess shear relationship. For the sediment model calibration, the transport functions are adjusted by scaling factors, which are simple linear multipliers to the capacity equation.

TABLE 1 The transport functions used for sediment model calibration and the sediment grading that they were developed for.

Transport function formula	Sediment grading
Ackers and White (1973)	Sand-gravel
Engelund and Hansen (1967)	Sand
Laursen-Copeland (LC) (1968–1993)	Silt-gravel
Meyer-Peter and Müller (MPM) (1948–1975)	Sand-gravel
Toffaleti (1968)	Sand
MPM-Toffaleti	Sand-gravel
Yang (1973, 1984)	Sand-gravel
Wilcock and Crowe (2003)	Sand-gravel

The MPM transport function was calibrated using a critical mobility scaling factor, which affects not only the capacity but also the minimum flow at which water can move a grain class. Thus, it is inversely related to flow. Models were run with different critical mobility adjustments for the MPM transport function. The simulated sediment loads for CS1 were compared against the estimated sediment load based on the Helley-Smith sampling. The best result (965.8 kg day^{-1} m^{-1}, MAE = 0) was reached using a critical mobility factor of 1.128.

For the winter model, the best hydraulic model for the winter period was used as the base of the sediment models (with riverbed Manning's n 0.02, and ice roughness 0.01). The sediment model parameters were set as in the autumn sediment model. The Van Veen bed gradation data from autumn was used also for the winter sediment models. Again, different transport functions were tested during calibration. The modelled sediment load was compared with the sediment load calculated from Helley-Smith and LSPIV measurements at CS1 (Table 3).

The best result was reached using the LC (Laursen-Copeland) transport function. LC is based on Laursen's (1958) method that estimates a total sediment load predictor. Sediment transport is defined based on the hydraulic characteristics of mean channel velocity, flow depth and energy gradient and based on the sediment gradation and fall velocity. Copeland (1993) later extended the range of applicability to gravel-sized sediments. The formula is suitable for sediment sizes between 0.011 to 29 mm. The calibration of the LC transport function was continued following the same procedure as for the autumn sediment model. The image velocimetry -based sediment load data was favoured for calibration because all the initial winter sediment models simulated sediment load (0 to 16.8 kg day^{-1} m^{-1}) much closer to the load (45.8 kg day^{-1} m^{-1}) when compared to the Helley-Smith-based load estimation (352.4 kg day^{-1} m^{-1}). The best result (45.9 kg day^{-1} m^{-1}, MAE = 0.1) was reached using a critical mobility factor of 0.724.

The best sediment models were further tested by running the autumn model with 1) winter discharge and autumn water level data and 2) winter discharge and water level data. Similarly, the winter model was run with 1) autumn discharge and winter water level and 2) autumn discharge and water level data. Thereby, the aim was to more thoroughly assess the autumn and winter models. All models were run with the calibrated MPM (critical mobility scaling factor 1.128) and LC (critical mobility scaling factor 0.724) transport

TABLE 2 The results of initial transport function calibration for autumn sediment models. Sediment load calculated from Helley-Smith samples (H-S) vs modelled load in cross-section CS1 and the mean absolute error (MAE). The transport function that estimated the load closest to the measured load is bolded.

Transport method	H-S, kg day^{-1} m^{-1}	Model, kg day^{-1} m^{-1}	MAE
Ackers-White	965.8	164419.0	163453.2
Engelund-Hansen		3023.6	2057.8
Laursen-Copeland		81019.3	80053.5
Meyer Peter Muller		**1082.0**	**116.2**
Toffaleti		6511.5	5545.7
MPM-Toffaleti		7432.5	6466.7
Yang		5724.9	4759.1
Wilcock-Crowe		3818.8	2853.0

TABLE 3 The results of initial transport function calibration for winter model. Sediment load calculated from Helley-Smith samples (H-S) and LSPIV measurements vs modelled load in cross-section CS1, and the mean absolute error (MAE). The transport function that estimated load closest to the measured load is bolded.

Transport function	HS, kg day^{-1} m^{-1}	Model, kg day^{-1} m^{-1}	MAE, H-S	MAE, LSPIV
Ackers-White	352.4	0	−352.4	−45.8
Engelund-Hansen		0.9	−351.5	−44.9
Laursen -Copeland		**16.3**	**−336.1**	**−29.5**
Meyer Peter Muller		0	−352.4	−45.8
Toffaleti	**LSPIV, kg day^{-1} m^{-1}**	0.1	−352.3	−45.7
MPM-Toffaleti	45.8	0.1	−352.3	−45.7
Yang		0.2	−352.2	−45.6
Wilcock-Crowe		0	−352.4	−45.8

functions. The autumn models that used the winter discharge data resulted in zero sediment transport with both transport functions. On the contrary, the winter models considering the autumn discharge greatly over-estimated the sediment load (sediment load with MPM 600 kg day^{-1} m^{-1} and with LC 86853 kg day^{-1} m^{-1}).

2.7 | Modelling of long-term observed min and max ice conditions on sediment transport

The most acceptable model to estimate the sediment load during ice-cover was selected to model the sediment load in different ice scenarios at Pulmanki based on long-term observations of minimum and maximum ice conditions. The most acceptable model used the LC transport function with the critical mobility adjusted to 0.724. The difference between the modelled sediment load and the image-based estimation was 0.1 kg day^{-1} m^{-1}. The ice thickness data was collected during 2014–2021 and consisted of average ice thickness values at CS1. Minimum and maximum ice-cover thicknesses were related to the ice thickness in 2021 and the multipliers (1.4046 [max], 0.8914 [min]) were used to calculate the ice thickness at each cross-section for minimum and maximum ice condition scenarios. Sediment models were run with the same settings as the most suitable model based on the calibration (section 2.6). Only the ice-cover data was changed to correspond to either the maximum, minimum or no ice conditions.

3 | RESULTS

3.1 | The results of the uncertainty analysis modelling and the impact of a variety of calibration data sets on model results

All initial sediment models estimated a significantly greater sediment load for autumn and a lower sediment load for winter than observed (Tables 2 and 3). For the autumn model, the best results were gained using MPM as the transport function. The best calibration results (i.e., the minimum difference between modelled and observed load) were reached using the transport function scaling factors, i.e., critical mobility factor. The closest model estimations to the measured sediment load were reached with an MPM critical mobility scaling factor of 1.128 (Table 4). The difference between modelled and measured load was 0 kg day^{-1} m^{-1}.

For the winter data, the models could not be acceptably calibrated to the measured load by Helley-Smith; modelled loads remained much lower (Table 3). The image-based sediment load estimation was reached using the LC transport function (with an adjusted critical mobility scaling factor of 0.724). The difference between modelled and image-based load estimation was 0.1 kg day^{-1} m^{-1}.

Calibrating the autumn models with the winter discharge data resulted in zero-modelled sediment transport with both transport functions (i.e., LC and MPM). In contrast, winter models calibrated with autumn discharge observations greatly over-estimated the sediment load (sediment load with MPM 600 kg day^{-1} m^{-1} and with LC 86853 kg day^{-1} m^{-1}) (Table 5).

3.2 | The spatial sediment transport in low-flow autumn open-channel and winter ice-covered flow conditions with morphodynamic models

The autumn and winter sediment transport conditions differed significantly as the sediment load at CS1 was 20-fold in autumn compared to winter (Figure 3). The difference was even greater at cross-sections CSA, CS2 and CSC. Flow velocities in the meander bend were much higher and variable in autumn (mean cross-sectional velocity range 0.042–0.520 ms^{-1}) than in winter when the mean cross-sectional velocities remained almost constant (0.036–0.087 ms^{-1}) (See Appendix, Table A5). In both seasons, velocities slowed down after the first cross-sections. In open-water conditions, this reduction in flow velocity was more prominent after CSB (from 0.085 to 0.087 ms^{-1}). Shear stress followed the pattern of velocity in both seasons (Appendix, Table A5). Within the meander bend, the locations of high and low transport conditions differed between the seasons, because in autumn the transfer accumulated until CS2 (highest sediment load 4,826 kg day^{-1} m^{-1}) and in winter the highest transport was modelled at CS1 (sediment load 46 kg day^{-1} m^{-1}). The lowest sediment loads were simulated within the meander bend with 46 kg day^{-1} m^{-1} at CS4 during autumn open-water conditions and no load simulated at CSC and CS4 during mid-winter ice-covered conditions.

The spatial variation of erosional and depositional locations in the meander bend varied with season (Table 6). In open-water conditions, erosion occurred at CSA and CS2 and deposition occurred at all other

TABLE 4 Summary of the sediment model performance with different transport functions and calibration data against observed sediment loads at CS1.

	Transport function	Modelled sediment load, kg day^{-1} m^{-1}		Transport function calibration method		Observed sediment load, kg day^{-1} m^{-1}		Difference (modelled-observed load), kg day^{-1} m^{-1}			
								H-S		LSPIV	
		Default	Adjusted	Scaling factor	Critical mobility	H-S	LSPIV	Def.	Adj.	Def.	Adj.
Autumn open-water	MPM	1082.0	965.8	x	1.128	965.8	x	116.2	0	x	x
Winter ice-cover	Laursen-Copeland	16.3	45.9	x	0.724	352.4	45.8	−336.1	−306.5	−29.5	0.1

TABLE 5 The simulated sediment loads from the test models. The test models were run with the other seasons discharge (Q) and water level (WL) data. Meyer Peter Muller (MPM) and Laursen-Copeland (LC) were used as transport functions.

	Autumn model		Winter Q, autumn WL		Winter Q, winter WL	
Transport function	MPM	LC	MPM	LC	MPM	LC
Sediment load kg day^{-1} m^{-1}	965.8	x	0	15.1	0	0
	Winter model		**Autumn Q, Winter WL**		**Autumn Q, Autumn WL**	
Transport function	MPM	LC	MPM	LC	MPM	LC
Sediment load kg day^{-1} m^{-1}	x	45.9	613.7	86853.0	600.0	86853.0

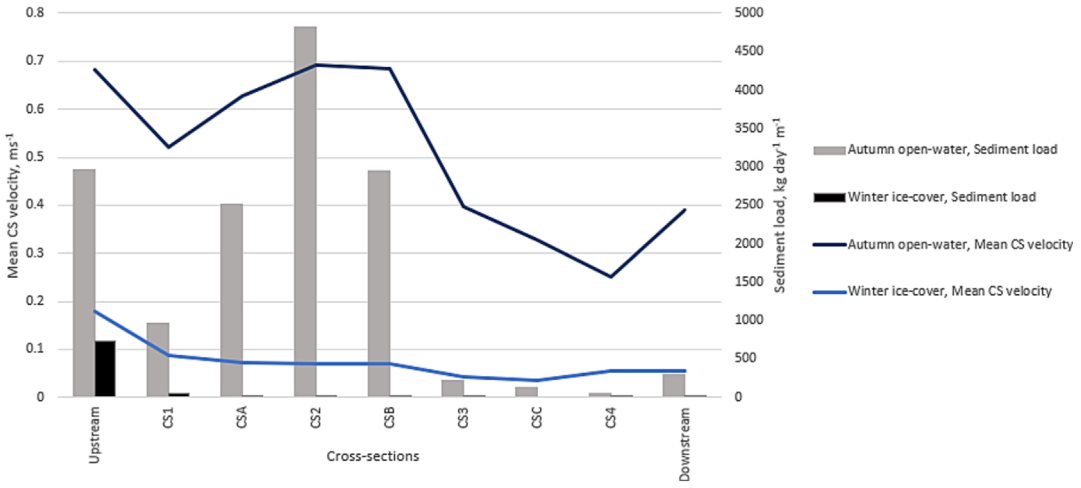

FIGURE 3 The spatial variation of sediment load and mean cross-sectional (CS) velocity based on autumn open-water and winter ice-cover models.

TABLE 6 Sediment transport (incoming [mass in] and outgoing [mass out] sediment load) and the most prominent processes in each cross-sections in autumn open-water and winter ice-covered conditions.

	Open-water conditions				Ice-covered conditions			
Cross-section	Mass in, kg day^{-1} m^{-1}	Mass out, kg day^{-1} m^{-1}	Difference	Process	Mass in, kg day^{-1} m^{-1}	Mass out, kg day^{-1} m^{-1}	Difference	Process
CS1	1286.0	965.7	320.2	deposition	258.2	45.9	212.3	deposition
CSA	1406.6	2517.0	−1110.4	erosion	49.7	17.0	32.7	deposition
CS2	4062.3	4826.1	−763.7	erosion	27.1	7.0	20.2	deposition
CSB	6528.0	2946.1	3581.9	deposition	10.1	5.3	4.8	deposition
CS3	1511.5	226.8	1284.7	deposition	3.2	0.5	2.7	deposition
CSC	183.5	121.6	61.9	deposition	0.4	0	0.4	deposition
CS4	159.3	45.7	113.6	deposition	0	0	0	-

cross sections. In ice-covered conditions, deposition was the main process in the meander bend.

3.3 | The impact of different winters on the bedload transport in a subarctic river

The increase or decrease of ice-cover thickness impacted flow velocity, sediment transport and shear forces (Figures 4 and 5, Table A6). While the discharge was kept constant for the different ice-cover scenarios, velocity, sediment transport and shear stress were mainly impacted by the changes in the under-ice space in the channel (Figure 6). Thus, during maximum ice thickness flow velocity, sediment transport and shear stress in the meander bend were significantly greater than in simulations using measured ice conditions. During minimum ice thickness, all parameters were lower than in simulations considering measured ice thicknesses. When the ice-cover was removed, velocity and shear forces were lower in ice-covered conditions and the sediment load in the meander bend was almost non-existent (Figure 4, Table A6). The differences between measured and minimum ice conditions were much smaller than between measured and maximum conditions. The spatial trend for each variable was similar between measured and minimum ice conditions. However, the spatial variation of these variables was different during maximum ice conditions, because the highest peaks of flow velocity, sediment transport and shear stress for maximum ice simulations were observed at CS1 and CSA (max velocity 0.243 ms^{-1}, sediment transport 1,318 kg day^{-1} m^{-1} and shear stress 0.099 Pa). During minimum and measured ice conditions, the overall trend for sediment load was decreasing in the modelled area from upstream until cross-section CSC.

4 | DISCUSSION

4.1 | The influence of model calibration data

Sediment transport models were calibrated to simulate sediment load in low-flow open-water conditions during autumn and in ice-covered conditions during mid-winter. The models for both seasons were calibrated with relatively small adjustments. The calibrated models performed well indicated by similar modelled and observed sediment load at CS1 in autumn and by only 0.1 kg day^{-1} m^{-1} more modelled than the observed load in winter (Table 4). Thus, errors in the model estimations were minor. Generally, the initial models (i.e., prior to transfer function calibration) estimated the load to be significantly higher in autumn and lower in winter than the field measurements. This indicates that the available transport function formulas, at least with their default settings, may not be sufficient to account for the complex processes governing sediment transport in natural rivers with fine sandy sediments. Thus, it is important to account for all uncertainties related to the model throughout the model calibration and to ensure that the acceptability of the model is not sacrificed for the search of the statistically best-performing model (Beven, 2006).

The LC transport function produced the best formulas, i.e., model structure, to be used for the winter conditions, but greatly overestimated the load for greater discharges during autumn (Tables 2 and 5). The LC formula allows the critical mobility factor to be adjusted. We found it to be a reliable transport function for winter models when the critical shear in the formula was decreased by 27%. Also, Sisinggih et al. (2020) reported good model performance when reducing the critical shear in the LC function for a simulation of sediment flushing in the Wlingi Reservoir in Indonesia. LC has been used successfully to estimate sediment transport in fume experiments (Talreja, Yadav, & Waikhom, 2013). The rather simplistic MPM transport function performed best in open water conditions (autumn) but failed to model any sediment load when the discharge was as low as measured in winter. However, when the winter models were run with the autumn discharge, the MPM predicted sediment load up to 600 kg day^{-1} m^{-1}. These results indicate that modelling sediment transport in different seasons and discharges requires a careful selection of transport functions suitable for the prevailing conditions. Even in the same river segment and with the same bedload gradation data the seasonal variation of discharge, ice and temperature will affect the equations needed for a robust sediment transport modelling.

Field measurements in winter are done through drillholes in ice, and thus measurements from under ice can be tedious to obtain resulting in point measurements only (Demers, Buffin-Belanger, &

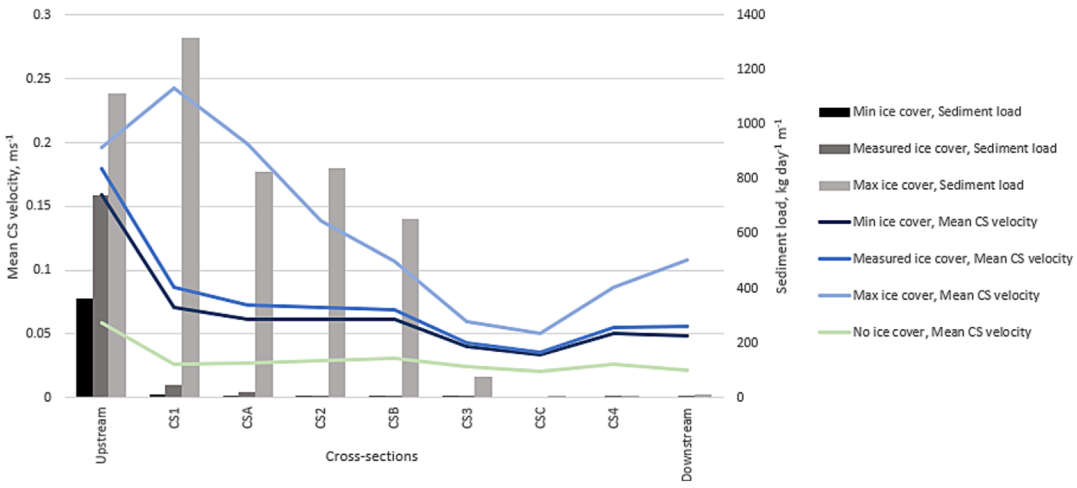

FIGURE 4 Spatial variation of sediment load and mean cross-sectional (CS) velocity in the model area simulated using different ice thicknesses (minimum, measured, maximum and no ice-cover).

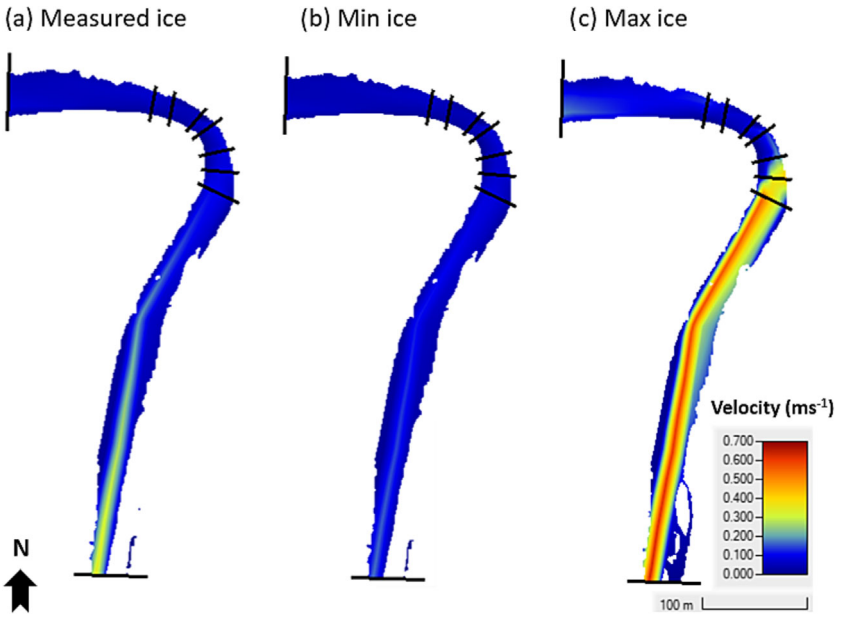

FIGURE 5 Spatial variation of modelled flow velocities in different ice thicknesses: a) measured ice, b) minimum ice and c) maximum ice. The black lines represent the cross sections.

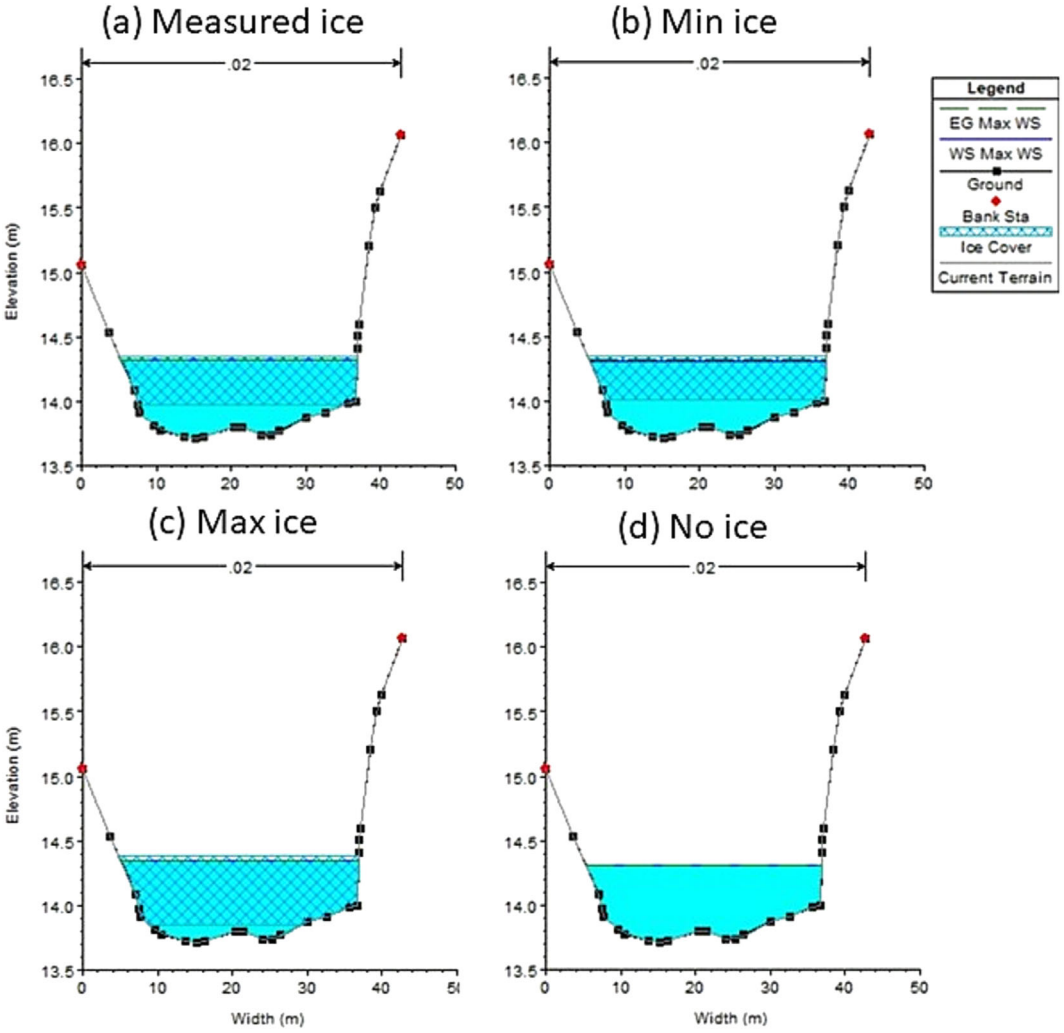

FIGURE 6 A visualization of the ice-cover and water level conditions in cross-section CS1 in different ice thickness scenarios: a) measured ice, b) minimum ice, c) maximum ice and d) no ice-cover.

Roy, 2011; Lotsari et al., 2017; Polvi et al., 2020). Especially sediment sampling can be challenging. To tackle this problem, we tested whether the model calibration could be enhanced using the image-based calculations of sediment transport as calibration data. The image-based velocity measurement and the photogrammetric 3D reconstruction methods are suitable for clear water conditions.

Therefore, they have great potential to estimate more accurately the sediment transport in low-flow conditions during autumn and winter. The image-based estimation of sediment transport (45.8 kg day^{-1} m^{-1}) in winter was significantly lower than those calculated with the Helley-Smith sampler (352.4 kg day^{-1} m^{-1}). It also enabled the final sediment model to be calibrated more accurately and with fewer adjustments, because the initial models systematically, largely under-estimated sediment loads at CS1. Another fact that justifies the usage of image-based over-Helley-Smith calibration data is the circumstance that hydraulic and trap-efficiency tests of the Helley-Smith sampler showed over-registration in streams carrying sand-sized material (Helley & Smith, 1971). The equipment was designed originally for flow regimes carrying materials of particle sizes between 2 and 10 mm and at velocities up to 3.048 ms^{-1}. However, this sampler has long been the best available mechanical equipment for simple bedload sampling. Thus, during both Pulmanki river conditions in autumn and winter, an overestimation of the Helley-Smith data would be expected. Therefore, we also used the image-based approach to estimate sediment transport in winter and to test whether the models could meet either or both sediment reference data sets. As our results show, the image-based method shows less sediment transport than the mechanical measurements as expected (Helley & Smith, 1971). Therefore, we would state that image-based measurements have the potential to become a more trustworthy method. We are currently performing more analyses to adapt image velocimetry methods for sediment load sampling.

Despite the great potential of LSPIV in sediment transport estimations, some caution should be taken. There are several factors that increase the uncertainties of the mean velocity measurements. The interaction between video settings, mainly frame rate and resolution and LSPIV settings (search window size) have a significant effect on the tracking values and it is difficult to visually recognize the optimal values. The accuracy of the orthoimage and digital elevation model, which was used to georeference the values, has a direct impact on the scaled velocity values (i.e., in ms^{-1}). Even though the accuracy of the orthoimage and digital elevation model was sufficient, the overall close-range application implies that small errors produce already large differences in calculated velocities. Overall, LSPIV tends to underestimate flow velocities (Tauro, Piscopia, & Grimaldi, 2017) and assumes that the whole flow area within the matching window has similar conditions, which is however not the case in this study. In such flow conditions tracking individual particles might be another option (Eltner, Sardemann, & Grundmann, 2020; Perks, 2020; Tauro et al., 2018).

4.2 | The spatial sediment transportation in low flow conditions

The magnitude of sediment transport and the locations of erosion and deposition differed significantly between open-water and ice-covered conditions. Flow velocities, shear stress and sediment transport were significantly lower in ice-covered river channels. This trend corresponds with earlier studies both in the laboratory (Ettema, Braileanu, & Muste, 2000; Lau & Krishnappan, 1985; Muste, Braileanu, & Ettema, 2000; Sayre & Song, 1979) and in natural rivers (Kämäri et al., 2015; Lotsari et al., 2019). Although, in this current study the seasonal variation was much greater than noted in previous studies. According to Turcotte et al. (2011), the sediment transport capacity of a river channel has been observed to decrease by 25–95% during ice-covered conditions, when compared to open-channel conditions. Comparing winter to autumn, our simulations resulted in a decrease in sediment load of 70–100%. However, the final sediment models were calibrated using sediment data derived from different methods, i.e., Helley-Smith in autumn and image velocimetry in winter. Therefore, the comparison should be made with caution as one of the sediment load estimations may represent the actual river conditions more accurately than the other.

The measured sediment load (based on Helley-Smith) at CS1 in autumn was 966 kg day^{-1} m^{-1} and the simulated loads for other cross sections ranged from 46 kg day^{-1} m^{-1} (CS4) up to 4,826 kg day^{-1} m^{-1} (CSB). In winter, the image-based sediment load measurement amounted 42 kg day^{-1} m^{-1}, whereas the simulation resulted in loads of up to 17 kg day^{-1} m^{-1} at other cross sections (CSA). CS3 and CS4 were completely depositional and no sediment load was estimated at these cross sections. As a comparison, Lotsari et al. (2014) measured bedloads ranging from 1,469 to 5,789 kg day^{-1} m^{-1} at the Tana River during high flow conditions in spring. Although the bedload in low flow conditions is expected to be lower, simulations in our study estimated sediment loads similar to the lowest range of Lotsari et al.'s (2014) measurements. The authors also concluded that the open-channel low flow period as a whole caused more sediment transport than the short spring-melt period. This further highlights the need for accurate and reliable methods to estimate sediment transport in low-flow open-water and ice-covered conditions.

From a spatial perspective, the locations of maximum flow, erosion and deposition varied between the simulated open-channel and ice-covered conditions, which corresponds with earlier studies (Lotsari et al., 2019). During winter, the flow velocity peaks at the beginning of the meander bend, at CS1, but further downstream flow velocity gradually slows down, shear stress decreases and sediment transport diminishes. Deposition is the main process in the meander bend. During autumn, flow velocity accelerates until CS1 and the highest flow, as well as the greatest shear stress, in the meander bend, occurs at CS1. Also, in autumn deposition is the prevailing process as erosion exceeds deposition only at cross sections CSA and CS2. According to previous studies (Demers, Buffin-Belanger, & Roy, 2011; Lotsari et al., 2017), the characteristics of flow in ice-cover conditions differ from those in open-water conditions as ice-cover increases the horizontal variation of the high-velocity region and the number and direction of stacked helical flows. Based on both simulation and measurement results, Lotsari et al., 2019 found that sedimentation was more likely to occur during ice-covered than in the open-channel conditions because ice-cover decreased the number of locations where critical velocities were exceeded. This is also the likely explanation of our simulation results.

4.3 | The influence of ice thickness on sediment transport

Simulations with different ice thicknesses resulted in either an increase (maximum ice thickness) or a decrease (minimum ice

thickness and no ice-cover) in sediment transport. In contrast to the sediment transport simulations with different ice-cover thicknesses in a river in south-western Finland (Kämäri et al., 2015), the model with maximum ice-cover thicknesses estimated increased flow velocities, shear stress and sediment transportation when compared to the model in our study using measured ice thicknesses. However, Kämäri et al. (2015) found that in some simulations, the ice narrowed the river channel causing the erosion to increase. Lotsari et al. (2019) also found areas in the river channel where flow in ice-covered conditions was greater than in open-water conditions in autumn. Robert & Tran (2012) displayed similar findings in a flume experiment. Thick ice occupies more space in the channel, narrowing the channel and potentially resulting in increased flow velocities, which again influence shear stress and erosion. In our simulation, this is very likely as the discharge was kept constant in the model but the ice-cover was increased.

The more area the ice-cover occupies the channel cross-section, the greater effect it has on flow characteristics (Ettema & Kempema, 2013) especially if the ice-cover is fixed and not affected by the flow (Ettema, 2002). In our simulation, minimum ice thicknesses resulted in slower flow velocities, lower shear stress and sediment transport compared to the model with measured ice-cover thicknesses, yet the difference was less distinct than between the simulations with measured and maximum ice thicknesses. The effective width of the river channel increased with decreased ice-cover providing more space for the discharge to pass. The flow and shear stress decreased even more when the ice-cover was removed, indicating that in ice-covered low-flow conditions ice-cover and its thickness alone have a significant effect on the sediment transport. Although our simulations with different ice thicknesses did not account for other factors (such as discharge and water temperature) that are altered in different climatic scenarios, these results highlight the effects of ice-cover and its properties on in-channel sediment transportation. Under climate change, bedload under ice-covered conditions could decrease, because of thinner ice but the annual sediment load is likely to increase as the ice-covered time period gets shorter and the precipitation increases.

5 | CONCLUSIONS

As climate change will be pronounced in high latitudes, it is crucial to understand the effects of hydroclimatic changes on annual sediment transportation in rivers that can be ice-covered for a vast period of the year. The study on spatial and temporal variation of the processes under ice-covered conditions in natural systems has thus far been challenging due to difficult observation conditions. However, novel approaches, such as photogrammetry and advanced hydro-morphological modelling, can provide more information in this field of study. Our study site represented a small (20-30 m wide) sand-bed river in a deglaciated environment. Such rivers are numerous in the circumpolar arctic and bring large amounts of sediment to the main rivers. Thus, the findings of our study are relevant to better understand the importance of these rivers for sediment delivery during different flow conditions, especially during ice-cover in winter. Our study supports previous observations of a substantial flow-driven decrease in sediment transport in ice-covered conditions when compared to open-channel conditions. Erosion is more pronounced in open-water, and thus, diminishing river-ice can be expected to decrease the under-ice sediment load in low flow conditions but increase the annual open-water sediment loads. Our simulations with different ice thicknesses demonstrated the importance of ice-cover on erosion and sediment transport because thick ice can substantially narrow the river channel causing an increase in flow velocity and erosion.

We stress the importance of good quality data to calibrate the hydro-morphodynamic models. The current transport function formulas used in morphologic modelling require adjustment and further development to be able to reach accurate estimates of sediment transport in cold deglaciated sandy river environments. Image-based estimates of sediment transport proved to enhance the model calibration. However, this flexible method needs further testing before traditional mechanistic and partly error-prone methods to measure sediment transport might be replaced. This paper is the first experiment on this matter. Our study reveals that the sediment transport equations and the calibration data might need fine-tuning. Thus, also modelling practices might need to be overall revised in a wider scientific community.

Finally, the open-access modelling software HEC-RAS has proven to be an efficient and reliable tool for 1D hydro-morphological modelling in ice-covered conditions. However, for a better understanding of sediment transport in ice-covered conditions, the development of 2D modelling with ice-cover is still much needed.

AUTHOR CONTRIBUTIONS

Pajunen V.: Leading writer, does the modelling, analyses the data sets and results, idea of the paper. Lotsari E.: Writing of the paper, ideas of the paper, Gladius Mini and GoPro measurements, and their planning and execution, long-term river ice, discharge and water level measurements, autumn 2020 and winter 2021 field measurements. Processing of bed load data sets. Funding for the project. Juha-Matti Välimäki: Juha-Matti Välimäki: Analysis of the bedload transport velocity from video data using particle image velocimetry and underwater photogrammetry. Franziska Wolff: Gladius Mini and GoPro underwater measurements, their planning and execution. Gathering the 2020 autumn data and processing of the 2020 autumn data sets. Marko Kärkkäinen (hired as assistant for HYDRO-RDI): processing of the field data. Especially processing of the topography data sets with SfM methods from the underwater photogrammetry and drone image, and bed load data sets. Linnea Blåfield: Measurement of winter 2021 bed load and discharge data. Measurement of long-term mid-winter discharge, ice-thickness and ice elevation data. Anette Eltner: processing of the UAV bathymetry field data from 2020 autumn and 2021 winter.

ACKNOWLEDGEMENTS

The ice-covered flow measurements were initiated under the post-doctoral research project of Dr. Lotsari, funded by the Academy of Finland (ExRIVER: grant number 267345). The work for this paper was supported financially also by other Academy of Finland-funded projects (DefrostingRivers: 338480; HYDRO-RDI: 337394 and 337279). The Academy of Finland and DAAD (Germany) also together supported the study financially via the mobility project "Hydro-morphological change detection of rivers in cold climate regions with

integrated spatiotemporal high-resolution methods" (332563). In addition, the Department of Geographical and Historical Studies, University of Eastern Finland, supported the work financially. The authors have no conflict of interest to declare. We would like to thank PhD Melanie Elias and Dr. Diana Spieler from Technische Universität Dresden for their valuable fieldwork assistance in 2020 autumn, and Prof. Petteri Alho and Dr. Carlos Gonzales-Inca from the University of Turku and Dr. Nikita Tananaev (Melnikov Permafrost Institute [MPI] at Yakutsk, Russia) for their valuable fieldwork assistance in 2021 winter. It would not have been possible to conduct the fieldwork without the drilling assistance of Ilkka Syvänperä from the Kevo Subarctic Research Institute of the University of Turku in 2021 winter. We thank Jutta Porkka for sieving the bulk bed sediment samples of the 2020 spring.

DATA AVAILABILITY STATEMENT

Data is available on request virpi.pajunen@aalto.fi.

ORCID

Virpi Pajunen https://orcid.org/0000-0002-5608-9353
Eliisa Lotsari https://orcid.org/0000-0002-0120-8722
Franziska Wolff https://orcid.org/0000-0002-6667-4169
Linnea Blåfield https://orcid.org/0000-0002-9126-2000
Anette Eltner https://orcid.org/0000-0003-2065-6245

REFERENCES

Ancey, C. & Pascal, I. (2020) Estimating mean bedload transport rates and their uncertainty. *Journal of Geophysical Research: Earth Surface*, 125(7), e2020JF005534. Available from: https://doi.org/10.1029/2020JF005534

Beven, K. (2006) A manifesto for the equifinality thesis. *Journal of Hydrology*, 320(1-2), 18–36. Available from: https://doi.org/10.1016/j.jhydrol.2005.07.007

Boyer, C., Verhaar, P.M., Roy, A.G., Biron, P.M. & Morin, J. (2010) Impacts of environmental changes on the hydrology and sedimentary processes at the confluence of St. Lawrence tributaries: potential effects on fluvial ecosystems. *Hydrobiologia*, 647(1), 163–183. Available from: https://doi.org/10.1007/s10750-009-9927-1

Brunner, G., Savant, G. & Heath, R.E. (2020) *Modeler application guidance for steady versus unsteady, and 1D versus 2D versus 3D hydraulic modeling*. U.S.A.: US Army Corps Engineers.

Copeland, R. (1993) Numerical Modeling of Hydraulic Sorting and Armoring in Alluvial Rivers, PhD Thesis, The University of Iowa, 284 p.

Demers, S., Buffin-Belanger, T. & Roy, A.G. (2011) Helical cell motions in a small ice-covered meander river reach. *River Research and Applications*, 27(9), 1118–1125. Available from: https://doi.org/10.1002/rra.1451

Demers, S., Buffin-Bélanger, T. & Roy, A.G. (2013) Macroturbulent coherent structures in an ice-covered river flow using a pulse-coherent acoustic Doppler profiler. *Earth Surface Processes and Landforms*, 38(9), 937–946. Available from: https://doi.org/10.1002/esp.3334

Eltner, A., Bertalan, L., Grundmann, J., Perks, M.J. & Lotsari, E. (2021) Hydro-morphological mapping of river reaches using videos captured with UAS. *Earth Surface Processes and Landforms*, 46(14), 2773–2787. Available from: https://doi.org/10.1002/esp.5205

Eltner, A., Sardemann, H. & Grundmann, J. (2020) Technical note: flow velocity and discharge measurement in rivers using terrestrial and unmanned-aerial-vehicle imagery. *Hydrology and Earth System Sciences*, 123 24(3), 1429–1445. Available from: https://doi.org/10.5194/hess-24-1429-2020

Ettema, R. (2002) Review of alluvial-channel responses to river ice. *Journal of Cold Regions Engineering*, 16(4), 191–217. Available from: https://doi.org/10.1061/(ASCE)0887-381X(2002)16:4(191)

Ettema, R., Braileanu, F. & Muste, M. (2000) Method for estimating sediment transport in ice-covered channels. *Journal of Cold Regions Engineering*, 14, 130–144. Available from: https://doi.org/10.1061/(ASCE)0887-381X(2000)14:3(130)

Ettema, R. & Kempema, E.W. (2013) Ice effects on sediment transport. In: Beltaos, S. (Ed.) *River ice formation*. Edmonton: Committee on River Ice Processes and the Environment, Canadian Geophysical Union, Hydrology Section, pp. 297–338.

Fujita, I., Muste, M. & Kruger, A. (1998) Large-scale particle image velocimetry for flow analysis in hydraulic engineering applications. *Journal of Hydraulic Research*, 36(3), 397–414. Available from: https://doi.org/10.1080/00221689809498626

Goede ED, Wagner T, de Graaff R, Sheets B. 2014. Modelling of Ice Growth and Transport on a Regional Scale. ASME, 33rd Int. Conf. on Ocean, Offshore & Arctic Eng., USA, p1–8.

Helley, E.J., Smith, W. 1971. Development and calibration of a pressure-difference bedload sampler. U.S. Geological Survey Open-File Report. U.S. Dept. of the Interior, Geological Survey, Water Resources Division: Menlo Park, California, USA. 18 p.

Hirvas, H., Lagerback, R., Mäkinen, K., Nenonen, K., Olsen, L., Rodhe, L., et al. (1988) The Nordkalott project: studies of quaternary ge-ology in northern Fennoscandia. *Boreas*, 17(4), 431–437. Available from: https://doi.org/10.1111/j.1502-3885.1988.tb00560.x

IPCC. (2021) In: Masson-Delmotte, V., Zhai, P., Pirani, A., Connors, S.L., Péan, C., Berger, S., *et al.* (Eds.) *Climate change 2021: the physical science basis. Contribution of working group I to the sixth assessment report of the intergovernmental panel on climate change*. UK: Cambridge University Press, In Press.

Kämäri, M., Alho, P., Aaltonen, J., Veijalainen, N., Huokuna, M. & Lotsari, E. (2015) River ice cover influence on sediment transportation at present and under projected hydro-climatic conditions. *Hydrological Processes*, 29(22), 4738–4755. Available from: https://doi.org/10.1002/hyp.10522

Kasvi, E., Alho, P., Vaaja, M., Hyyppä, H. & Hyyppä, J. (2013) Spatial and temporal distribution of fluvio-morphological processes on a mean der point bar during a flood event. *Hydrology Research*, 44(6), 1022–1039. Available from: https://doi.org/10.2166/nh.2013.091

Lau, Y. & Krishnappan, B. (1985) Sediment transport under ice cover. *Journal of Hydraulic Engineering*, 111(6), 934–950. Available from: https://doi.org/10.1061/(ASCE)0733-9429(1985)111:6(934

Laursen, E. M. (1958). The total sediment load of streams. *Journal of the Hydraulics Division*, 84(1), 1–36. Available from: https://doi.org/10.1061/jyceaj.0000158

Leopold, L.B., Wolman, M.G. & Miller, J.P. (1964) *Fluvial processes in geomorphology*. W.H. Freeman and company: San Fransisco and London, p. 522.

Ljubičić, R., Strelnikova, D., Perks, M.T., Eltner, A., Peña-Haro, S., Pizarro, A., et al. (2021) A comparison of tools and techniques for stabilising unmanned aerial system (UAS) imagery for surface flow observations. *Hydrology and Earth System Sciences*, 25(9), 5105–5132. Available from: https://doi.org/10.5194/hess-25-5105-2021

Lotsari, E., Dietze, M., Kämäri, M., Alho, P. & Kasvi, E. (2020a) 2020a macro-turbulent flow and its impacts on sediment transport potential of a Subarctic River during ice-covered and Open-Channel conditions. *Water*, 12(7), 1874. Available from: https://doi.org/10.3390/w12071874

Lotsari, E., Hackney, C., Salmela, J., Kasvi, E., Kemp, J., Alho, P., et al. (2020b) Sub-arctic river bank dynamics and driving processes during the open-channel flow period. *Earth Surface Processes and Landforms*, 45(5), 1198–1216. Available from: https://doi.org/10.1002/esp.4796

Lotsari, E., Kasvi, E., Kämäri, M. & Alho, P. (2017) The effects of ice cover on flow characteristics in a subarctic meandering river. *Earth Surface Processes and Landforms*, 42(8), 1195–1212. Available from: https://doi.org/10.1002/esp.4089

Lotsari, E., Lind, L. & Kämäri, M. (2019) Impacts of hydro-climatically varying years on ice development in a subarctic river. *Water*, 11(10), 2058. Available from: https://doi.org/10.3390/w11102058

Lotsari, E., Tarsa, T., Kämäri, M., Alho, P. & Kasvi, E. (2019) Spatial variation of flow characteristics in a subarctic meandering river in ice-covered

and open-channel conditions: 2D hydrodynamic modelling approach. *Earth Surface Processes and Landforms*, 44(8), 1509–1529. Available from: https://doi.org/10.1002/esp.4589

Lotsari, E., Veijalainen, N., Alho, P. & Käyhkö, J. (2010) Impact of climate change on future discharges and flow characteristics of the tana river, sub-arctic northern fennoscandia. *Geografiska Annaler: Series a, Physical Geography*, 92(2), 263–284. Available from: https://doi.org/10.1111/j.1468-0459.2010.00394.x

Lotsari, E., Wainwright, D., Corner, G.D., Alho, P. & Käyhkö, J. (2014) Surveyed and modelled one-year morphodynamics in the braided lower Tana River. *Hydrological Processes*, 28(4), 2685–2716. Available from: https://doi.org/10.1002/hyp.9750

Lotsari, E., Wang, Y., Kaartinen, H., Jaakkola, A., Kukko, A., Vaaja, M., et al. (2015) Gravel transport by ice in a subarctic river from accurate laser scanning. *Geomorphology*, 246, 113–122. Available from: https://doi.org/10.1016/j.geomorph.2015.06.009

Mosselman, E. (2012) Modelling Sediment Transport and Morphodynamics of Gravel-Bed Rivers. In: Church, M., *et al.* (Eds.) *Gravel-bed Rivers: processes, tools, environments*. John Wiley & Sons.

Muste, M., Braileanu, F. & Ettema, R. (2000) Flow and sediment transport measurements in a simulated ice-covered channel. *Water Resources Research*, 36(9), 2711–2720. Available from: https://doi.org/10.1029/2000WR900168

Oveisy A, Dibike YB, Prowse TD, Beltaos S, de Goede E 2015. 2DH numerical simulation of ice dynamics during break up. CGU HS CRIPE 18th Workshop, Hydraulics of Ice Covered Rivers, Canada

Peel, M.C., Finlayson, B.L. & McMahon, T.A. (2007) Updated world map of the Köppen-Geiger climate classification. *Hydrology and Earth System Sciences*, 11(5), 1633–1644. Available from: https://doi.org/10.5194/hess-11-1633-2007

Perks, M.T. (2020) KLT-IV v1.0: image velocimetry software for use with fixed and mobile platforms. 71(13), 6111–6130. Available from: https://doi.org/10.5194/gmd-13-6111-2020

Perks, M.T., Dal Sasso, S.F., Hauet, A., Jamieson, E., Le Coz, J., Pearce, S., et al. (2020) Towards harmonisation of image velocimetry techniques for river surface velocity observations. *Earth System Science Data Discussions*, 48(12), 1545–1559. Available from: https://doi.org/10.5194/essd-12-1545-2020

Polvi, L.E., Dietze, M., Lotsari, E., Turowski, J.M. & Lind, L. (2020) Seismic monitoring of a subarctic river: seasonal variations in hydraulics, sediment transport, and ice dynamics. *Journal of Geophysical Research: Earth Surface*, 125(7), e2019JF005333. Available from: https://doi.org/10.1029/2019JF005333

Prowse, T., Alfredsen, K., Beltaos, S., Bonsal, B., Duguay, C., Korhola, A., et al. (2011) Past and future changes in arctic lake and river ice. *Ambio*, 40(S1), 53–62. Available from: https://doi.org/10.1007/s13280-011-0216-7

Robert, A. & Tran, T. (2012) Mean and turbulent flow fields in a simulated ice-covered channel with a gravel bed: some laboratory observations. *Earth Surface Processes and Landforms*, 37(9), 951–956. Available from: https://doi.org/10.1002/esp.3211

Sayre WW, Song GB 1979. Effects of Ice cover on alluvial channel flow and sediment transport process. Iowa institute of hydraulic research. The University of Iowa, IIHR Report No. 218, Iowa City, Iowa; 96 pp.

Sisinggih D, Wahyuni, S., Nugroh, R., Hidayat, F., Rahman, K. I. 2020 Sediment transport functions in HEC-RAS 4.0 and their evaluation using data from sediment flushing of Wlingi reservoir - Indonesia IOP Conf. Series: Earth and Environmental Science 437 012014 IOP. https://doi.org/10.1088/1755-1315/437/1/012014

Smith BT, Ettema R. 1995. Ice-cover influence on flow and bedload transport in dune-bed channels. In IIHR Technical Report 374. Iowa Institute of Hydraulic Research, The University of Iowa: Iowa City.

Sontek. (2024). SonTek M9. Available from: https://ysi.com/sontek-m9 [Accessed 28th February 2024].

Sui, J., Wang, J., He, Y. & Krol, F. (2010) Velocity profiles and incipient motion of frazil particles under ice cover. *International Journal of Sediment Research*, 25(1), 39–51. Available from: https://doi.org/10.1016/S1001-6279(10)60026-1

Talreja, J., Yadav, S.M. & Waikhom, S. (2013) Estimating the sediment transport capacity using HEC-RAS. *Global Research Analysis*, 2, 2277–8160.

Tauro, F., Piscopia, R. & Grimaldi, S. (2017) Streamflow observations from Cameras: large-scale particle image velocimetry or particle tracking velocimetry? *Streamflow from Cameras: LSPIV or PTV?* 203(53), 10374–10394. Available from: https://doi.org/10.1016/j.eats.2017.03.019

Tauro, F., Piscopia, R., Grimaldi, S., Tosi, F., Mattoccia, S. & Toth, E. (2018) Optical tracking velocimetry (OTV): leveraging optical flow and trajectory-based filtering for surface streamflow observations. *Remote Sensing*, 10(12), 2010. Available from: https://doi.org/10.3390/rs10122010

Thielicke, W., Stamhuis, E.J., 2014. PIVlab – Towards User-friendly, Affordable and Accurate Digital Particle Image Velocimetry in MATLAB. 4 2. https://doi.org/10.5334/jors.bl

Tsai W-F, Ettema R. 1996. A study of ice-covered flow in an alluvial bend. IIHR Technical Report 376. Iowa Institute of Hydraulic Research, The University of Iowa: Iowa City.

Turcotte, B., Morse, B., Bergeron, N.E. & Roy, A.G. (2011) Sediment transport in ice-affected rivers. *Journal of Hydrology*, 409(1-2), 561–577. Available from: https://doi.org/10.1016/j.jhydrol.2011.08.009

US Army Corps of Engineers. 2021. HEC-RAS 1D Sediment Transport Technical Reference Manual. Version 6.1. Hydrologic Engineering Center, Davis. USA.

Verhaar, P.M., Biron, P.M., Ferguson, R.I. & Hoey, T.B. (2011) Implications of climate change in the twenty-first century for simulated magnitude and frequency of bed-material transport in tributaries of the saint-Lawrence River. *Hydrological Processes*, 25(10), 1558–1573. Available from: https://doi.org/10.1002/hyp.7918

Zanke, U. & Roland, A. (2020) Sediment bed-load transport: a standardized notation. *Geosciences*, 3(10), 368. Available from: https://doi.org/10.3390/geosciences10090368

SUPPORTING INFORMATION

Additional supporting information can be found online in the Supporting Information section at the end of this article.

How to cite this article: Pajunen, V., Lotsari, E., Välimäki, J.-M., Wolff, F., Kärkkäinen, M., Blåfield, L. et al. (2024) The impacts of low flow, ice-cover and ice thickness on sediment load in a sub-arctic river – Modelling sediment transport with particle image velocimetry calibration data sets. *Earth Surface Processes and Landforms*, 1–15. Available from: https://doi.org/10.1002/esp.5809